

# The T2K Side Muon Range Detector (SMRD)

S. Aoki<sup>e</sup>, G. Barr<sup>h</sup>, M. Batkiewicz<sup>d</sup>, J. Błocki<sup>d</sup>, J.D. Brinson<sup>f</sup>, W. Coleman<sup>f</sup>, A. Dąbrowska<sup>d</sup>, I. Danko<sup>i</sup>, M. Dziewiecki<sup>m</sup>, B. Ellison<sup>f</sup>, L. Golyskin<sup>b</sup>, R. Gould<sup>f</sup>, T. Hara<sup>e</sup>, J. Haremza<sup>f</sup>, B. Hartfiel<sup>f</sup>, J. Holeczek<sup>j</sup>, A. Izmaylov<sup>b</sup>, M. Khabibullin<sup>b</sup>, A. Khotjantsev<sup>b</sup>, D. Kietczewska<sup>l</sup>, A. Kilinski<sup>g</sup>, J. Kisiel<sup>j</sup>, Y. Kudenko<sup>b</sup>, N. Kulkarni<sup>f</sup>, R. Kurjata<sup>m</sup>, T. Kutter<sup>f</sup>, J. Łagoda<sup>g</sup>, J. Liu<sup>f</sup>, J. Marzec<sup>m</sup>, W. Metcalf<sup>f</sup>, C. Metelko<sup>k</sup>, P. Mijakowski<sup>g</sup>, O. Mineev<sup>b</sup>, D. Naples<sup>i</sup>, M. Nauman<sup>f</sup>, T.C. Nicholls<sup>k</sup>, D. Northacker<sup>i</sup>, J. Nowak<sup>f</sup>, M. Noy<sup>a</sup>, V. Paolone<sup>i</sup>, G.F. Pearce<sup>k</sup>, O. Perevozchikov<sup>f</sup>, M. Posiadała<sup>l</sup>, P. Przewłocki<sup>g</sup>, W. Qian<sup>k</sup>, M. Raymond<sup>a</sup>, J. Reid<sup>f</sup>, E. Rondio<sup>g</sup>, E. Shabalin<sup>b</sup>, M. Siyad<sup>k</sup>, D. Smith<sup>f</sup>, J. Sobczyk<sup>n</sup>, M. Stodulski<sup>d</sup>, R. Sulej<sup>g</sup>, J. Świerblewski<sup>d</sup>, A.T. Suzuki<sup>e</sup>, T. Szegłowski<sup>j</sup>, M. Szeptycka<sup>g</sup>, M. Thorpe<sup>k</sup>, T. Wachała<sup>d</sup>, D. Warner<sup>c</sup>, A. Weber<sup>k</sup>, T. Yano<sup>e</sup>, N. Yershov<sup>b</sup>, A. Zalewska<sup>d</sup>, K. Zaremba<sup>m</sup>, M. Ziembicki<sup>m</sup>

<sup>a</sup>Imperial College London, Physics Department, London, United Kingdom

<sup>b</sup>Institute for Nuclear Research, Moscow, Russia

<sup>c</sup>Colorado State University, Department of Physics, Fort Collins, Colorado, USA

<sup>d</sup>H. Niewodniczański Institute of Nuclear Physics PAN, Kraków, Poland

<sup>e</sup>Kobe University, Department of Physics, Japan

<sup>f</sup>Louisiana State University, Department of Physics & Astronomy, Baton Rouge, Louisiana, USA

<sup>g</sup>National Centre for Nuclear Research, Warsaw, Poland

<sup>h</sup>University of Oxford, Department of Physics, Oxford, United Kingdom

<sup>i</sup>University of Pittsburgh, Department of Physics and Astronomy, Pittsburgh, Pennsylvania, USA

<sup>j</sup>University of Silesia, Institute of Physics, Katowice, Poland

<sup>k</sup>STFC Rutherford Appleton Laboratory, Harwell Oxford, United Kingdom

<sup>l</sup>University of Warsaw, Institute of Experimental Physics, Warsaw, Poland

<sup>m</sup>Warsaw University of Technology, Institute of Radioelectronics, Warsaw, Poland

<sup>n</sup>Wrocław University, Institute of Theoretical Physics, Wrocław, Poland

arXiv:1206.3553v1 [physics.ins-det] 15 Jun 2012

## Abstract

The T2K experiment is a long baseline neutrino oscillation experiment aiming to observe the appearance of  $\nu_e$  in a  $\nu_\mu$  beam. The  $\nu_\mu$  beam is produced at the Japan Proton Accelerator Research Complex (J-PARC), observed with the 295 km distant Super-Kamiokande Detector and monitored by a suite of near detectors at 280m from the proton target. The near detectors include a magnetized off-axis detector (ND280) which measures the un-oscillated neutrino flux and neutrino cross sections. The present paper describes the outermost component of ND280 which is a side muon range detector (SMRD) composed of scintillation counters with embedded wavelength shifting fibers and Multi-Pixel Photon Counter read-out. The components, performance and response of the SMRD are presented.

**Keywords:** Neutrinos, neutrino oscillation, T2K, muon range detector, scintillation counter, wavelength shifting fiber, multi-pixel photon counter, readout electronics

## 1. Introduction

The Tokai to Kamioka (T2K) experiment is a second generation long-baseline accelerator neutrino oscillation experiment[1, 2, 3] which started taking data in January 2010. The principal goal of the project is to measure neutrino oscillation parameters by searching for the appearance of electron neutrinos ( $\nu_e$ ) in a beam of muon neutrinos ( $\nu_\mu$ ) and by performing precision measurements of the muon neutrino disappearance. The project utilizes protons from the new 30 GeV Main Ring (MR) proton synchrotron at J-PARC in Tokai[3] to produce a  $\nu_\mu$  beam on a stationary graphite target. A 295 km distant detector at Kamioka is placed  $2.5^\circ$  off-axis to measure beam neutrinos. The upgraded water Cherenkov detector, Super-Kamiokande[1, 4], serves as far detector for T2K. The use of an off-axis beam results in a neutrino energy spectrum that is narrowly peaked at about 600 MeV corresponding

to the oscillation maximum for a baseline of 295 km. The off-axis configuration also leads to a significant reduction in backgrounds originating from a beam intrinsic electron neutrinos. The estimated fraction of electron neutrinos at the peak energy is  $\nu_e/\nu_\mu \sim 0.4\%$ . A near detector complex at J-PARC is used to monitor the neutrino beam, measure neutrino event rates and to help minimize systematic uncertainties in the measurements of neutrino oscillation parameters. A detector facility is located 280 m downstream from the target was built at J-PARC in Tokai for this purpose. Neutrino oscillation parameters can be derived from flux and spectral measurements of  $\nu_\mu$  and  $\nu_e$  performed with the Super-Kamiokande and with the near detectors. The near detectors provide a normalization of the unoscillated flux and a measurement of backgrounds. The near detector complex houses two detectors[5, 6]: an on-axis interactive neutrino grid detector (INGRID) and an off-axis near detector, ND280 [1, 7]. Protons are accelerated up to 30 GeV and proton spills

are successively extracted every 3.5 seconds from the J-PARC main ring synchrotron into the neutrino beamline. The neutrino beamline leads to a graphite target[10] onto which neutrinos impinge. The target is embedded in the first of three magnetic horns which are excited by a pulsed current that is synchronized with the beam. During (anti-)neutrino runs the horns serve to focus (negatively)positively charged pions into a 96 m long decay volume, where they decay into muons and muon neutrinos. The neutrino beam direction needs to be tuned and monitored precisely since for an off-axis configuration the peak neutrino energy changes by 2% per millirad change in beam direction. The neutrino beam flux and direction is measured by the on-axis INGRID detector which is composed of an array of iron-scintillator sandwich detectors. The off-axis detector ND280 is positioned at a  $2.5^\circ$  off-axis angle as is the far detector and it's primary purpose is to measure the unoscillated neutrino energy spectrum, the  $\nu_e$  contamination in the beam and neutrino interaction cross sections. The dominant neutrino interaction process around the T2K neutrino peak energy of about 600 MeV is charged-current quasi-elastic (CC-QE) scattering  $\nu_\mu n \rightarrow \mu^- p$ . The CC-QE cross-section measured by ND280 will be used as a reference cross-section for measurements in the Super-Kamiokande detector. In order to achieve the projected sensitivities [2] of the experiment, the momentum resolution of muons from CC-QE interactions should be better than 10% [2]. The expected precision for determining the energy scale is better than 2% and the backgrounds for a  $\nu_e$  appearance should be measured with uncertainties smaller than 10% .

## 2. The Off-axis Detector and the SMRD

The off-axis near detector ND280 consists of finely segmented detectors which act as neutrino targets and tracking detectors and are surrounded by an electromagnetic calorimeter (ECal) and a magnet which houses a side muon range detector (SMRD). The inner part of the detector is divided into multiple regions: a  $\pi^0$  detector (P0D), a tracking detector which in turn consists of two fine grained detectors (FGD) made from scintillators and water modules and three gaseous time projection chambers (TPC). The layout of the detector is shown in Fig. 1.

The P0D detector consists of scintillator planes interleaved with lead, brass and water layers. It is designed to measure backgrounds for the electron neutrino appearance search in the far detector. In particular the background from the neutral current reaction with only a single  $\pi^0$  in the final state and the electron neutrino contamination in the beam. Segments with water are implemented for neutrino water cross-section measurements.

Downstream of the P0D is the tracking detector which is optimized to measure momenta of charged particles, particularly muons and electrons and recoil protons produced in charged current quasi-elastic interactions. The tracking detector consists of two fine grained detectors which are interspersed with three time projection chambers. The FGDs provide the target mass for neutrino interactions in the tracker. Directions and ranges of short tracks such as recoil protons produced by CC-QE interactions in the FGD are measured. The first FGD mod-

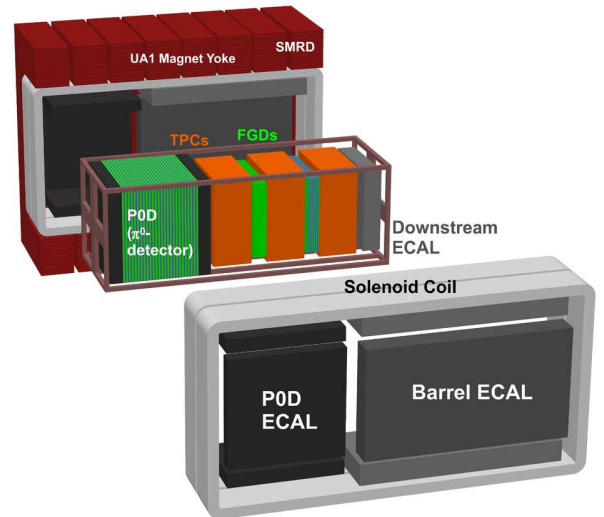


Figure 1: A view of the ND280 off-axis detector.

ule is made of layers which in turn are composed of scintillator bars with perpendicular orientation from one layer to the next. The second module consists of equivalent scintillator bars which are interspersed with passive water layers to allow for cross section measurement on water. The primary purpose of the TPC is to measure muon and electron momenta for neutrino energy reconstruction in CC-QE interactions and ionization energy losses,  $\frac{dE}{dx}$ , for particle identification.

Both P0D and tracker are surrounded by an electromagnetic calorimeter to detect showering ( $e^-$ ,  $\gamma$ ) particles which escape from the tracking detector and P0D and allow for better event reconstruction and particle identification. The inner part of the off-axis detector is placed inside the UA1 dipole magnet, which is operated to produce a uniform horizontal magnetic field of 0.2 T. The magnet yoke is divided into two halves, each made of eight C-shaped flux return yokes. Each of these individual yokes consists of sixteen iron plates, 48 mm thick, and spaced with 17 mm air gaps.

The side muon range detector consists of a multiple layers of plastic scintillation counters placed in the air gaps in between the iron plates which make up the yokes of the UA1 magnet. The main purpose of the SMRD is to measure muon momenta for muons which are created in neutrino interactions and which escape the inner detectors at large angles with respect to the neutrino beam. It also serves to identify backgrounds from beam neutrino interactions in the magnet yoke and surrounding walls and to provide a cosmic trigger signal for calibration purposes of the ND280 detector. A detailed description of the ND280 near detector can be found in [1].

One of the main goals of the ND280 detector is to measure the neutrino energy spectrum. For charged current quasi elastic CC-QE processes, neutrino energy is closely related to the muon momentum and its angle of emission. The active target mass is concentrated in the FGD and P0D detectors. Muons emitted at large angles with respect to the neutrino beam di-

rejection often leave short or no tracks in the TPC. Such muons will intersect the ECal as well as the SMRD and the iron yokes surrounding the entire detector. Their momenta can be inferred from the range in iron and the SMRD measurements. The directions of muons can be determined based on information from the inner detectors and the position information in the plastic scintillation counters of the SMRD.

Estimates based on MC studies indicate that a significant fraction of all muons which originate from CC-QE reactions intersect the SMRD. The vast majority of large angle muons which does not escape in the forward direction, e.g. for  $\cos \theta > 0.8$ , have momenta of less than 600 MeV/c. Muons with energies less than 600 MeV will range out within less than 350 mm of iron. The iron plates of magnet yokes are 48 mm thick and hence it is sufficient to instrument 6 to 7 radial layers in order to range out the majority of muons that are not escaping in the forward direction.

The principal requirement for the SMRD detector is to detect particles with very high efficiency. Hence the active detector medium has to enclose the inner detectors nearly hermetically and provide uniform efficiency across the entire sensitive area. An additional requirement is the long-term stability of all detector components to ensure good performance and longevity over the lifetime of the experiment. The SMRD will also be used to identify backgrounds entering the detector from outside as well as from interactions of beam neutrinos in the iron of the magnet yoke. The SMRD provides the trigger signal in response to through-going cosmic ray muons. These muons are an invaluable calibration source for the inner detectors as they provide a sample of muon tracks that are, apart from their direction, very similar to the muons created in neutrino beam interactions.

### 3. SMRD Hardware

The side muon range detector is embedded in the former UA1 and NOMAD magnet which is now located at J-PARC in Tokai, Japan. The magnet is housed in a 17 m deep detector pit without overburden, 280m downstream from the carbon target and at an off-axis angle of  $2.5^\circ$ . The following sections describe the geometry, design and components of the SMRD.

#### 3.1. The ND280 Off-Axis Magnet

The former UA1 magnet consists of 16 flux return yokes which are grouped in pairs (labeled 1 through 8 from upstream to downstream with respect to the neutrino beam direction) to form a series of 8 consecutive rings which surround the magnetic field and the current coils on four sides. All 16 yokes have essentially the same dimensions with the four yokes forming the first and the last ring exhibiting slightly different geometry at the interface where two yokes meet to form a ring. The nominal outer dimensions of each yoke are 6150mm  $\times$  2815mm  $\times$  876mm (height  $\times$  width  $\times$  depth) and the enclosed space measures 4040mm  $\times$  3600mm  $\times$  7568mm (height  $\times$  width  $\times$  depth). The relative ring spacing amounts to 110 mm for the outermost rings and 80 mm for all other rings. The original UA1 inner volume width was 80mm smaller but the yokes were slightly

modified for the NOMAD experiment. Each yoke is composed of sixteen 48mm thick iron plates which are separated by 17mm thick spacers and held together by long bolts. Figure 2 shows the basic structure of a single yoke and the slits in between iron plates. Slits which are located in between the same set of bolts form a group labeled as tower. Except for corner towers, all

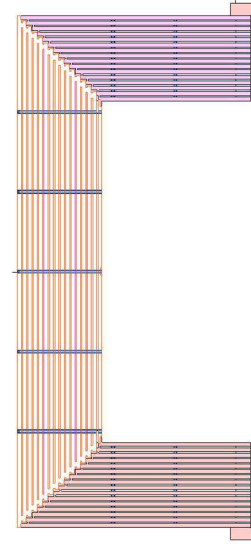


Figure 2: Engineering drawing view of a single yoke. A series of bolts hold the iron plates together and sub-divide each yoke into 4 horizontal, 4 vertical and 2 corner sections.

horizontally oriented slits have a nominal gap size of 17mm  $\times$  700mm  $\times$  876mm (height  $\times$  width  $\times$  depth), and all vertically oriented slits have a nominal gap size of 910mm  $\times$  17mm  $\times$  876mm (height  $\times$  width  $\times$  depth). Due to imperfections and deformations of the magnet as well as welding seams of the spacers the actual gap sizes may differ slightly.

#### 3.2. The SMRD

Each yoke consists of 16 iron plates which are spaced at a distance of 17mm which leads to a set of 15 slits in radial direction. Active detector components, populate the three innermost gaps in all yokes so as to be able to detect particles escaping the inner detectors. Particles which escape the inner detectors on the sides have slightly higher mean energy compared to particles which are exiting through the top or bottom where the magnet coil material causes additional energy loss. Therefore, additional active layers have been installed in the sides of the most downstream yokes; a total of 4 vertical layers in yoke 6 and 6 layers in yokes 7 and 8. The location of the larger number of layers of active detector material was chosen to maximize the observation of muons originating from beam related neutrino interactions inside ND280.

The SMRD consists of 192 horizontally oriented and 248 vertically oriented detector modules in total. The external dimensions of the detector modules are dictated by the dimensions of the slits in the yokes and measure to 9mm  $\times$  686mm  $\times$  955mm (height  $\times$  width  $\times$  depth) for horizontal and 9mm  $\times$

892mm × 955mm (height × width × depth) for vertical modules. The module height is pointing radially outward and the module depth is parallel to the long axis of the magnet. The counter sizes have been optimized to maximize the active area in each magnet slit. Due to the differently sized spaces for horizontal and vertical slits, horizontal SMRD modules are composed of 4 scintillation counters with dimensions 7mm × 167mm × 875mm (height × width × length) and vertical SMRD modules consist of 5 scintillation counters with dimensions 7mm × 175mm × 875mm (height × width × length). Hence, the SMRD consists of 768 horizontal and 1240 vertical scintillation counters in total.

Polystyrene-based scintillator slabs, each with an embedded wave-length shifting (WLS) fiber, serve as active elements for the SMRD detector. The WLS fiber is read out on both ends to increase light yield, improve uniformity and position accuracy, and provide redundancy (Fig. 3). A key feature of the individual

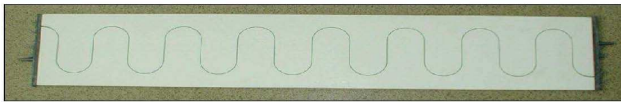


Figure 3: SMRD scintillator slabs with a serpentine-routed Y11 WLS fiber.

SMRD counters is the usage of a serpentine-shaped fiber. The design results in near uniform response across the surface of the scintillation counter [8] and minimize the number of photosensors and electronics channels compared to more conventional designs with multiple straight fibers. Extruded polystyrene scintillators (1.5% PTP, 0.01% POPOP) have been produced by Uniplast, a company in Vladimir, Russia. The outer surfaces of each slab are etched by a chemical agent, thus resulting in formation of a white diffuse layer. The deposit thickness is 30-100 μm depending on etching time. The diffuse layer acts as a reflector and has been demonstrated to increase the light yield by 40 to 50% relative to a scintillation counter without such a diffusively reflective layer. The advantage of the approach is an almost ideal contact of the reflector with the scintillator. Details about the extrusion technique and the method of etching a scintillator with a chemical agent can be found in [13]. Extruded scintillators of this type have shown good light yield stability over at least two years [14]. After the etching procedure raw scintillator slabs were cut with a milling machine and the serpentine-shaped groove was milled successively. For the SMRD counters the serpentine geometry of a groove consists of 15 half-circles, each with a diameter of 58 mm and straight sections connecting the semi-circles. Due to the different widths of horizontal and vertical counters grooves of two different lengths are required: 2.10 m for horizontal counters and 2.22 m for vertical ones. The groove depth is 2.8 mm and deepens to 3.55 mm towards both ends of the counters so as to allow the fiber to exit the scintillator at mid-height. Grooves were milled in multiple passes with a 1.1 mm diameter mill to ensure good optical surface properties of the grooves. The accuracy of the milling operation was 100 μm. A 1 mm diameter Y11 (150) Kuraray WLS fibers of flexible S-type and with double-cladding [15] was used

for the SMRD counters. Fibers are bent into a serpentine-shape and glued into grooves with BC600 Bicon glue. Details of the gluing technique are described in [12].

The long term stability of bent WLS fibers was tested with two photosensors MRS APDs [16] and a blue LED as a light source. Several 3 m long fiber samples were wound into 7 turns to reproduce similar bending stresses. A bending diameter of 60 mm led to an average initial drop in light transmission quality of about 5%, which is in a good agreement with Kuraray data [15]. The light attenuation was measured as the ratio of the light signal at the far fiber end to the signal at the close end. The near end signal served as a reference of LED intensity. A straight fiber of the same length was used to calibrate the photosensors. No degradation in light attenuation other than the initial decrease has been observed over a period of more than a year. In the SMRD scintillation counters the WLS fiber exits both sides of the scintillator through a ferrule which is part of a custom made endcap. Endcaps are glued and screwed to the end faces of each scintillator counter, and are injection molded and made out of black vectra, a brand of liquid crystal polymer and which was tested to be light tight at the few photon level. Each endcap features a snap-on mechanism to engage a connector with an inserted Hamamatsu multi pixel photon counter (MPPC) [17], to couple to the endcap and the WLS fiber ferrule, respectively. The MPPCs are backed by a foam spring to ensure a reliable coupling between the photosensor front face and the polished WLS fiber ends. Figure 4 shows an engineering drawing of the connector containing a photosensor and clipped to the endcap.

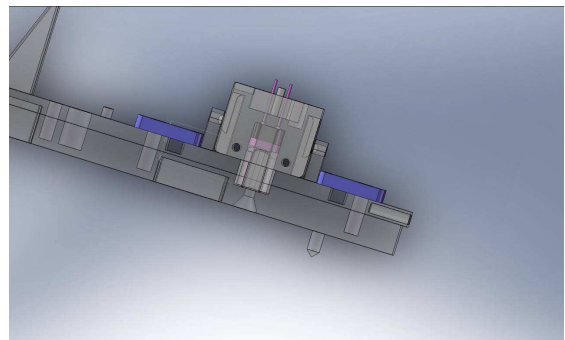


Figure 4: Partial view of a SMRD scintillator counter endcap with the optical connector housing a MPPC and a mini PCB.

All 4016 MPPCs of the SMRD are connected to miniature printed circuit boards (PCB) which are free to slide along rails in the backside of the optical connector. The free movement of the PCB along the leads of the photosensors ensures good optical connections between WLS fiber and MPPC and averts damage to the MPPC front face due to overpressure. The miniature PCBs couple the MPPC signals into Hirose mini-coax cables which lead the signals to the Trip-t frontend boards (TFBs) [18, 19]. The front end electronics is mounted on the vertical sections of the magnet yokes. The mini coax-cables are routed between the magnet yokes and measure 3.5m and 3.0m for horizontal modules and are 2.2m long for all vertical modules.

### 3.3. Photosensors

Multi Pixel Photon Counters (MPPC) [17] developed for T2K by Hamamatsu were chosen as the common photosensor for all ND280 scintillator based detectors. Key features of these devices are their insensitivity to magnetic fields and their compact size which make them well suited for applications near or in the magnetic field and within the limited space available inside the UA1 magnet. The total number of MPPCs used for the SMRD amounts to 4016.

The custom made version of the MPPCs for T2K consist of an array of 667 independent  $50 \times 50 \mu\text{m}^2$  avalanche photodiodes (pixels) operating in Geiger mode. The MPPC sensitive area of  $1.3 \times 1.3 \text{ mm}^2$  is well suited to accept light from a 1 mm diameter Y11 fiber. The MPPC signal is a sum of pixel avalanches and this multi-pixel sensor operates as an analog photodetector with a dynamic range that is limited by the finite number of pixels. Typical light signals in SMRD counters are below 50 photoelectrons and therefore dynamic range issue are not a concern. Each pixel can be represented as a microcapacitor which quickly discharges during Geiger breakdown initiated by a photoelectron until the voltage difference across it has decreased below the breakdown voltage. The overvoltage, which is defined as the difference between the supplied bias voltage and the breakdown voltage, is the main parameter that affects the performance of MPPCs and the stability of its operation. MPPCs have an excellent single photoelectron resolution up to mean charges corresponding to about 30 photoelectrons that allow to perform an accurate calibration of each counter.

At a temperature of  $T = 25^\circ\text{C}$  and an overvoltage of 1.6 V MPPCs are characterized by a typical gain of  $7.5 \times 10^5$ , a photo detection efficiency of about 25% for green light as emitted by a Y11 fiber. The average dark rate amounts to 700 kHz with maximum values approaching up to 1 MHz, the estimated combined crosstalk and afterpulse probability is 20-25% and the recovery time of a single pixel is 30 ps. The MPPCs of the SMRD were operated in the T2K neutrino beam starting in 2009 and after more than 1.5 years of operation only one sensor (0.025%) is suspected to have failed. All MPPCs were tested extensively as function of bias voltage and temperature and in particular the gain and dark rate had to satisfy stringent criteria in order for a MPPC to be included in the SMRD.

### 3.4. Module Assembly and Installation

At multiple stages of the detector production and assembly the performance of the scintillation counters with embedded WLS fiber were tested in response to cosmic rays. First, the scintillators were tested immediately after the extrusion process by measuring the light yield with a photomultiplier tube and in response to throughgoing muons. Secondly, after the endcaps were attached to the scintillation counters and the WLS fiber had been glued into the grooves with BC600 optical glue the counters were retested using MPPCs and double ended readout in response to central penetrating muons. Out of 2008 counters 20 were found to have a large asymmetry (more than 50%) in light yield between the two ends. The asymmetry was attributed to a damages of the fiber cladding incurred during the

gluing process. These 20 counters were repaired by gluing a new fiber into a refurbished groove after milling out the previously glued fiber. All counters which passed the quality test, were wrapped by one layer of 0.1 mm thick Tyvek paper which leads to a further increase in light yield of 15%.

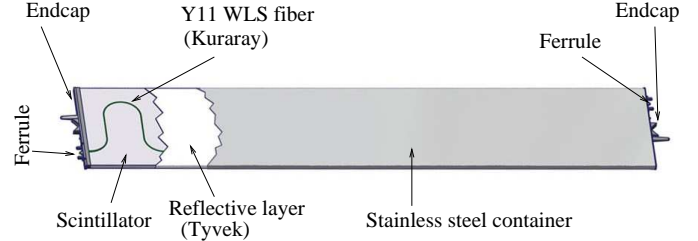


Figure 5: SMRD counter sliced view.

Successively the counters were wrapped in a lightproof stainless steel container (Fig. 5). The container was attached to scintillator and endcaps with DP-490 black epoxy glue and a double sided  $20 \times 0.15 \text{ mm}$  Tesa adhesive tape. Additionally all joints between the container surface and the endcap were covered by a black Tesa adhesive tape of  $25 \times 0.065 \text{ mm}$ . Each fiber end inside the endcap ferrule was cut by a cylindrical mill and polished to provide good optical contact with the MPPC. After assembly, the dark noise of each SMRD counter was measured with MPPCs and an oscilloscope to ensure the absence of light leaks. In total, 2130 counters ( $800 - 167 \text{ mm}$  wide and  $1330 - 175 \text{ mm}$  wide counters) were assembled and tested to be of good quality. After shipment to Japan 230 counters were found to have developed a sub-millimeter sized air gap between the end of the fiber and the face of the ferrule, resulting in a small loss in light yield. Hence the endcaps of all counters were additionally fastened by 2 stainless steel screws each in order to minimize the risk of future counter degradation. After refurbishment of the problematic counters all counters were re-tested and demonstrated to show excellent performance.

Single counters are assembled into bigger units named modules to facilitate installation and to stabilize the position of the counters in the magnet slits. In order to match the different dimensions of vertical and horizontal magnet slits two types of SMRD modules were built. Modules intended for vertical slits consist of five counters (each  $175 \text{ mm}$  wide) while the horizontal ones consist of four counters (each  $167 \text{ mm}$  wide). Extruded Aluminum H-profiles are used to inter-connect counters into modules. The boundary edges of the first and last counter in each module were protected with aluminium U-channels as shown in fig. 6. The counters and the extrusions are tightly wrapped with capton tape in three locations. In order to stabilize a module inside a magnet slit tape springs made of phosphorbronze are mounted on both sides of the modules as indicated in Fig. 7. Two springs are mounted on each side of the vertical modules while three per side are attached to the H-profiles of horizontal modules. Any lateral and longitudinal forces from the springs act on the H-profiles and not on the counters or endcaps whose interconnection is considered to be the most sensitive part of a detector module. The springs are

900 mm long, 15 mm wide, 0.4 mm thick. Each tape spring has 5 waves. The shapes of the springs are symmetric to ensure proper module positioning during installation in the magnet. Both ends of each aluminium extrusion are tapered (right panel of Fig. 7) to facilitate the installation process. The final

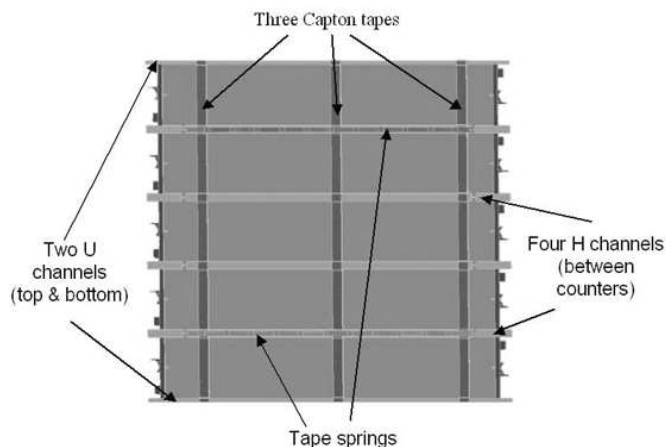


Figure 6: Scheme of the vertical SMRD module.

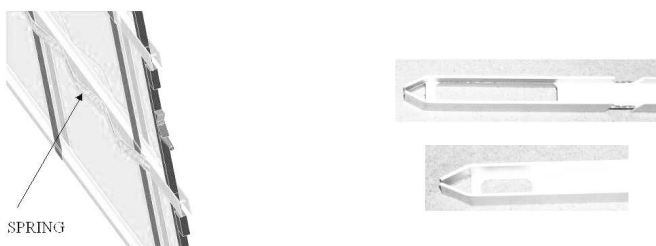


Figure 7: Springs mounted and fixed on Hprofiles (left), tapered end of C and H-profiles (right).

assembly and installation of the 248 vertical and 192 horizontal SMRD modules was performed at J-PARC between February and June 2009. A photo of a SMRD horizontal module is shown in Fig. 8.

SMRD modules were inserted into the magnet slits from the front and back face of the magnet and slid to their final positions. Each module was tested for possible damages during installation by reading out photosensor signals immediately after positioning it in its final location. After the completion of installation and checks protective covers were installed on the front faces of the magnet to prevent any damages to SMRD modules.

### 3.5. Counter Quality Assurance and Pre-installation Tests

Quality assurance (QA) of all SMRD counters was carried out at multiple stages throughout the production process. The light yield of raw scintillator slabs was tested in response to penetrating cosmic muons and with a photomultiplier attached for readout. After machining the S-shaped groove and gluing



Figure 8: Completed SMRD horizontal module equipped with photo-sensors and combined power and signal cables.

of a WLS fiber counters were tested with cosmic muons passing through an area of  $7 \times 7 \text{ cm}^2$  in the central area. In order to assure good response of the counters for an anticipated experiment lifetime of 10 years the light yield requirement for the sum of both ends measured at  $20^\circ\text{C}$  is more than 25 p.e. per minimum ionizing particle (MIP). Quality assurance measurements show the light yield to range from 25 to 50 p.e./MIP (Fig. 9). For centrally penetrating muons differences in signal

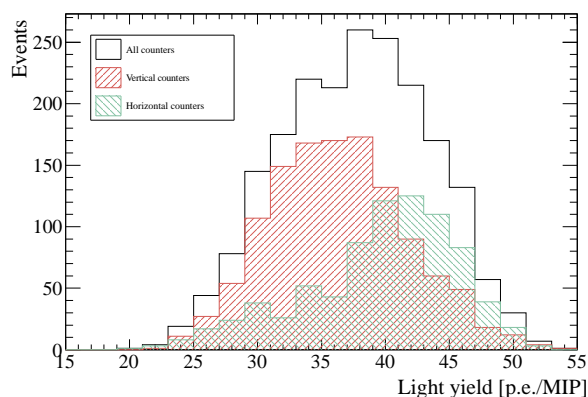


Figure 9: The light yield distribution for 2024 SMRD counters (including 16 spares).

sizes at both counter ends are required to be less than 20% so as to guarantee near uniform response and no fiber damage. Less than 1% of the counters were rejected but passed the quality assurance after a new WLS fiber had been inserted (see section 3.4).

The performance of all SMRD counters with attached MPPC photo-sensors was measured again after shipment and assembly into modules. A small  $2 \times 2 \text{ cm}^2$  muon telescope was placed at the center of each counter and used to trigger signal readout on both ends of the SMRD counters. The mean light yield for the sum of both ends was near 40 p.e./MIP after subtraction of MPPC cross-talk and after-pulses. The mean detection efficiency for minimum ionizing particles was in excess of 99.9%.

The temperature during the performance tests was in the range from 20.5 to 22.5°C and the bias voltages of both MPPCs were set to 68.7 V. In addition, the timing resolution of counters, defined as the uncertainty on  $(T_{left} - T_{right})/2$  was measured as function of light yield (Fig. 10). For a light yield of 40 p.e. a time resolution of 0.9 ns was achieved. The position resolution

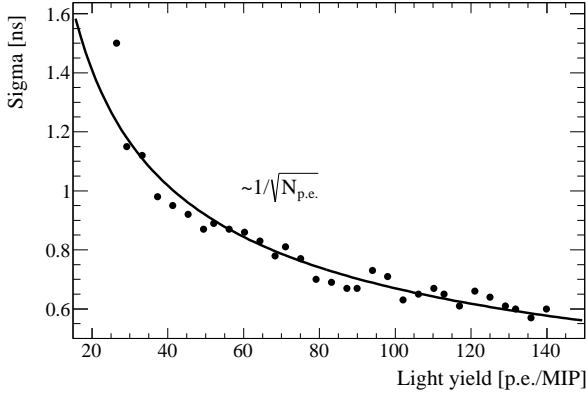


Figure 10: Time resolution of a SMRD counter versus light yield (after time-walk correction). The data are recorded in response to cosmic muons penetrating the center of the scintillator slab.

of a counter along its major axis based on both time difference between signals at both counter ends and the charge asymmetry between the signals was estimated and found to be of order of 8.5 cm.

### 3.6. Electronics and Power Requirements

The electronics for the SMRD is based on the TRIP-t ASIC developed at Fermilab[18]. It is the same electronics as used by some of the other sub-detectors of the T2K near detector. For an overview of the near detector complex and its components see [1].

Signals from up to 64 MPPCs are routed to custom designed front end boards (TFB: TRIP-t Front-end Board) that house 4 TRIP-t ASICs using miniature coax cables. The signals from the photosensors are capacitively split and routed to separate channels of the ASIC to increase the dynamic range of the electronics. A one photo-electron (p.e.) signal corresponds to around 10 ADC counts in the high gain channel, while the full scale signal in the low gain channel corresponds to 500 pe.

The TRIP-t chip is integrating the charge in programmable integration windows, which are synchronized with the neutrino beam structure. There is a programmable reset time after each integration cycle, which is at least 100 nsec long. The chip can store the result of 23 integration cycles in a capacitor array. Once the 23 integration cycles have been recorded, the data is multiplexed onto two dual channel 10-bit ADCs, which digitize the data. Signals from the high gain channel are routed to a discriminator, which is part of the TRIP-t ASIC. The front-end board is controlled by an FPGA, which timestamps the data with a precision of 2.5 ns. The threshold to generate a timestamp is programmable from 0 to 5 p.e. The ADC and timestamp

data is assembled by the FPGA and send to a backend board for data concentration and buffering. The output of the discriminators are also used to calculate trigger primitives, which are used to initiate the readout of the detector for cosmic ray muons. One normally requires hits from both ends of a scintillator counter within a 23 ns coincidence window and at least 2 counters to be hit, before a trigger primitive is transmitted to the cosmic trigger module. Monitoring information of temperature and MPPC bias voltages are also recorded by the TFB and asynchronously transmitted to the RMM. More detail of the front end part of the electronics can be found in [19].

The backend of the electronics system consists of four readout merger modules (RMMs), a cosmic trigger module (CTMs), one slave clock module (SCM) and a master clock module (MCM). All the boards have a common hardware platform, which has been build around a high end Vertex II Pro FPGA from Xilinx, which is clocked at 100 MHz. The board can drive 14 high speed optical links via its RocketIO and up to 192 LVDS links.

The signals from 128 TFBs, which are mounted on the detector and up to 3.5 m away from the photosensors, are routed to the four RMMs via cat5e cables. Each RMM controls 32 TFBs, distributes the clock and trigger signals and receives the data after a trigger signal was received by the TFBs. It asynchronously sends data via Gigabit Ethernet link to a commercial PC that collects and processes the data. Each RMM is equipped with 500 MByte DDR2 memory and can buffer up to 128 triggers. The RMMs receive trigger and timing signals from the SCM.

The MCM receives signals from the accelerator that determine when the neutrino spill happens and also from a GPS based clock. The GPS signals are used to synchronize the electronics to coordinated universal time (UTC). The MCM is also connected to the cosmic trigger module (CTM), which receives signals from up to 192 TFBs. All 128 TFBs used to read out the SMRD are set up to contribute to the generation of cosmic triggers. Readout is initiated, if at least 2 TFBs reading out data on two different sides of the detector are generating a trigger primitive in a 200 nsec window. The CTM is highly configurable. The trigger primitives can be prescaled, to suppress some combinations of SMRD walls or towers, e.g. to allow a cosmic muon event sample with preferentially horizontal directions. The prescale factors are set using an 8-bit word. All timing and trigger signals are transmitted via a RocketIO driven optical link from the MCM to the SCM.

The power requirements for the TFBs and RMM/CTMs are listed in table 1. Eight TFBs are mounted on the vertical side of each magnet yoke. All TFBs are mounted, evenly spaced, onto 6063 Aluminum architectural C-Channel that spans the entire vertical height of the magnet yokes. The C-channel is electrically isolated from the magnet steel to reduce the possibility of noise pickup. In addition to structural support for the TFB mounting, the inside of the C channel itself is used for power cable routing and strain relief.

Power to the TFBs is distributed by a system of power distribution panels. Two primary power panels service one half of the magnet each. These panels are mounted on lower middle

section of the magnet and are directly connected to two Wiener PL508 power supplies located on a lower level. One primary panel connects via 10 AWG wire to 8 secondary power distribution panels which are mounted on the bottom of each yoke and C-Channel mounting rail. Each secondary power panel services 8 TFBs and the power to each TFB is supplied using 22 AWG wire. The voltages for each secondary panel are fused: 5 A fuse for 1.7 V, 7.5 A fuse 3.1 V, 1 A fuse for 3.8 V and 2 A fuse for 5.5 V. In case of an electrical short on one of the TFBs at most 8 TFBs will lose voltage. The power to the 4 RMMs and CTM are supplied and fused (7.5 A fuse for both 3.1 V and 3.8 V and 1 A fuse for 5.5 V) at the primary power distribution panels.

Power Requirements		
Voltage(V)	Current(A)	
	per TFB	per RMM/CTM
1.7	0.24	–
3.1	0.60	1.0
3.8	0.05	6.0
5.5	0.18	6.0

Table 1: Power requirements per TFB and RMM or CTM. The SMRD uses a total of 128 TFBs, 4 RMMs and 1 CTM.

### 3.7. Data Acquisition System

The SMRD is configured and read out by a global T2K ND280 data acquisition (DAQ). It is based on the MIDAS DAQ framework [25] operating on commercially available computing hardware running the Scientific Linux operating system. MIDAS is interfaced to the experimental hardware through custom C/C++ front-end client applications.

The SMRD electronics is read out and controlled by the DAQ front end processor nodes (FPN) which are interfaced to the back-end electronics modules (RMMs) by point-to-point optical gigabit Ethernet links. Each FPN serves up to two back-end boards. The FPN is implemented as three tasks running as separate processes, interconnected by shared memory data buffers and communicating via standard inter-process mechanisms. Readout and configuration of the electronics and all connected hardware is provided by the readout task (RXT). The readout is parallelised across electronics boards in a multi-threaded manner and data is buffered for access by the data processing task (DPT). The RXT additionally receives periodic monitoring data from the TFBs and external temperature sensors which it passes to the global slow control. The DPT performs data reduction and basic data processing. The DPT decodes the TFB raw data blocks, associates amplitude and timing information for individual hits, performs pedestal subtraction on a channel-by-channel basis, applies zero-suppression to the unsparsified data and formats the data for output. To preserve monitoring information, the DPT also performs per-channel histogramming of signal amplitudes for specific trigger types prior to zero suppression and periodically inserts the histograms into the output data stream. The processed event fragments are buffered and dispatched to the DAQ back-end by the

third process, which implements the MIDAS front-end functionality.

The MIDAS framework provides the core components necessary for the DAQ system and is used to gather the event fragments from the SMRD FPNs (and from the other ND280 sub-detectors). An event building process collects the fragments, performs basic consistency checks and writes the fully assembled events to a system buffer for output by a logger process to a local RAID array. A custom archiver process transfers completed files to a mass storage facility over the network and additionally makes a preview copy to a local semi-offline system for fast-turnaround analysis.

### 3.8. Data Monitoring

A custom online-monitoring (OM) server based around the ROOT framework retrieves built events from the system buffer and generates a range of plots for data and detector quality monitoring as well as diagnostic alarms. The online monitoring allows to perform real time and near online data checks of the SMRD. The ND280 online monitoring framework is derived from the consumer monitor package developed for the Collider Detector at Fermilab (CDF) [20] and is integrated into the ND280 software framework and directory structure. The data monitoring system receives events from the data acquisition (DAQ) system. It analyzes the data stream of events and outputs results in the form of histograms, tables, and warnings.

The OM system consists of several data monitoring programs, one for each sub-detector of the ND280. Each of the programs connects to the DAQ and continually listens to a socket. Upon receipt of a set number of events or an end of run message it performs a diagnostic analysis of which the resulting histograms are saved to a file. The monitor functions are divided into 5 different levels according to the number of events and frequency required to perform the checks. Level 1 monitor functions act on an event by event level whereas level 5 functions accumulate data for one hour before being activated.

Multiple ROOT based viewer programs can connect from remote machines through a socket connection to a display server which has access to the information in the shared memory in real time. Using the display program, users can select and view multiple histograms of interests. For the SMRD the key parameters that are being monitored are the MPPC gain, dark rate and position and width of individual photo electron peaks for each channel which are derived from multi-Gaussian fits to the respective ADC spectra. Data are displayed in an intuitive and accessible format for user to be able to quickly identify problems. An error handler process receives warning and error messages from different monitoring programs, displays them with appropriate action required and has the ability to keep detailed logs. Alert range boundaries can be adjusted by means of a parameter settings file and without affecting the running of the monitor.

## 4. Detector Calibration and Performance

The calibration of the SMRD response is applied in two stages. The lower level calibration operates on individual pho-

tosensor signals and consist of procedures common for all Trip- $t$  based subsystems. The higher level calibration involves multi-channel, SMRD-specific operations which are presented in Sec. 4.2.

The low level calibration translates ADC signal amplitudes into charge values in units of photo-electron equivalent (p.e.). Both raw ADC values, from the low- and the high-gain output of the Trip- $t$  chip, are processed. After pedestal subtraction the two ADC values are combined with a polynomial function into a single, linearized  $ADClin$  value. The  $ADClin$  values are scaled according to the channel gain to obtain the charge amplitude in units of p.e. Pedestal and gain calibration constants are updated every 3 hours for all readout channels and stored in an online database which is common to all Trip- $t$  subsystems.

Signal timing is obtained from the TDC output of Trip- $t$  chips. Times correspond to the time an ADC signal surpasses a 4.5 p.e. threshold. The timing value in nanoseconds is calculated as  $t = 2.5 \times TDC \text{ bins}$  and aligned with a common reference time for all subsystems. Two charge-dependent effects influence the signal timing (*timewalk effect*). The first is related to the Trip- $t$  board electronics and arises from the exponential charging of the capacitors. It is corrected at the lower level of the calibration. The distribution of the time difference ( $\Delta t$ ) between signals observed at opposite ends of a counter is shown in figure 11. The distribution narrows from 12 ns to 9 ns after the correction. The second effect is caused by the light propagation in the scintillator and the WLS fiber which exhibit an exponential behavior. It causes a statistical signal timing delay in registering  $n$  photons out of a total number of  $N$  photons. The expected mean value of the delay is subtracted from the signal time and leads to a modest further reduction of the width of the distribution of time differences between signals at opposite ends (Fig. 11).

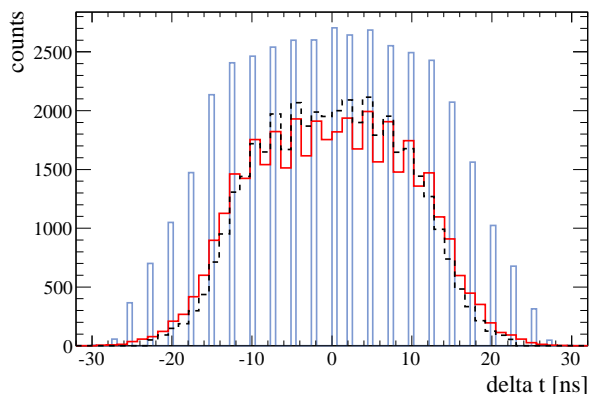


Figure 11: Signal time difference distribution without timewalk correction (solid blue,  $\sigma = 11.9$  ns), with electronics timewalk correction (solid red,  $\sigma = 9.5$  ns) and with full electronics and scintillation timewalk correction (dashed black,  $\sigma = 8.8$  ns).

#### 4.1. Counter Light Yield

The light yield of all scintillation counters is a critical performance parameter of the SMRD and as described in section

3.5 has also been used for quality assurance purposes during the manufacturing process. In test bench setups the SMRD counters showed light yields from 25 to 50 p.e. in response to cosmic muons penetrating the counter center perpendicularly to its surface. Asymmetries in signal sizes between the two ends were less than 20%. After installation of the SMRD counters into the UA1 magnet, cosmic ray data samples are used to measure the light yield for each counter. The light yield was determined using calibrated signals from both photosensors of each counter. The calibration corrects the signals for light attenuation in the WLS-fiber. Figure 12 shows distributions of the mean light yield for horizontal and vertical counters in response to cosmic muons that are predominantly vertical and horizontal, respectively. The cosmic muons have a near uniform distribution across the counter surface. The blue and red hatched histograms

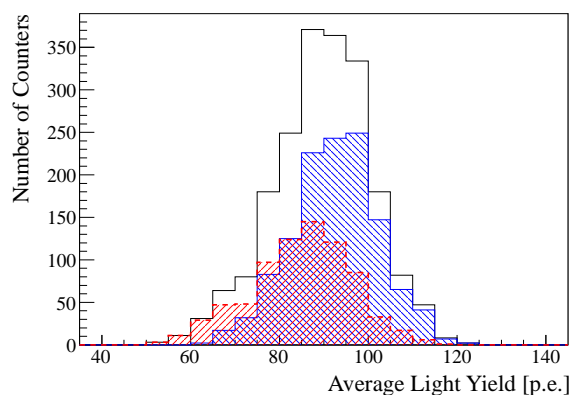


Figure 12: Mean light yield of horizontal and vertical SMRD counters in response to highly selective set of near vertical and near horizontal cosmic muons. Blue and red hatched histograms represent vertical and horizontal counters, respectively and the black histogram corresponds to all counters.

represent vertical and horizontal counters, respectively. The black histogram represents all counters. The mean value of the mean light yields amounts to 84 p.e. for horizontal counters and 92 p.e. for vertical counters. The difference in light yield for horizontal and vertical counters is partially due to mean muon pathlength differences in the counters caused by the angular distribution of cosmic muons. The mean light yields are also larger compared to the pre-installation test stand measurements. The differences can be attributed to the correction for light attenuation in the WLS fiber and differences in the counter illumination. All counters show good performance in response to uniformly distributed and near perpendicular muons. The stability of the light yield versus time is discussed in section 4.4.

#### 4.2. Timing Properties and Position Resolution

For each ADC signal with an amplitude larger than 4.5 p.e. an arrival time is recorded. The double sided readout of the SMRD counters therefore allows to determine the relative time difference between signals at each end of the counter and thus reconstruct the position of the particle initiating the scintillation light in the direction of the beam. Hit coordinates in the direction perpendicular to the beam,  $x_{hit}$  and  $y_{hit}$  are always set

to the middle of the scintillator slab since there is no position sensitivity in these directions.

Determination of the particle hit time ( $t_{hit}$ ) and successive position reconstruction along the counter ( $z_{hit}$ , e.g. in the direction of the beam) requires a signal at each end of the counter. Both signals are required to be above a threshold amplitude of 4.5 p.e. and within a 23 ns time coincidence window. The size of the coincidence window was chosen to minimize contamination from accidental noise coincidences without rejecting a significant fraction of good hit candidates. The estimated light propagation time for a signal to travel end to end in the embedded WLS fiber is 13 ns. Hence the chosen coincidence window leaves a margin for uncertainty in the timing measurement of individual signals (see Fig. 11). The particle hit time is obtained from the times of individual signals as

$$t_{hit} = t_{qmax} - \frac{l_z}{2v_{eff}} - \frac{1}{2}(\Delta t), \quad (1)$$

where  $t_{qmax}$  is the arrival time of the larger of the two signals,  $l_z$  is the length of the counter slab (876 mm),  $v_{eff}$  is the effective speed of light along the counter axis which is measured to be 65.5 mm/ns and  $\Delta t$  is the time difference between the arrival times of signals at both ends.

The z-hit position is evaluated w.r.t. the middle of the counter, and is calculated based on the signal timing difference and the charge asymmetry of the two signals. A two-stage Bayesian estimate is applied to combine the time and charge information optimally. A uniform prior probability distribution of the particle hit position is assumed since cosmic muons are expected to illuminate the counters uniformly. Successively the probability distribution for the particle hit position is constructed in two consecutive steps which are based on charge asymmetry and timing difference measurement information. The uncertainties of the time and charge measurements are taken into account as likelihood parameters. An evaluation of the probability distributions for arrival times and signal charges is implemented numerically in the off-line calibration software and results in a high granularity in hit position. The particle hit position bias and position uncertainty are taken from the resulting probability distribution as the mean value and standard deviation. Results of the position reconstruction for horizontal counters and cosmic muon data are shown in Fig. 13. The peak structure is caused by signal timing quantization. The resolution of the particle hit position reconstruction is at the level of 85 mm.

### 4.3. Counter efficiencies

The efficiencies of individual SMRD counters has been studied using cosmic trigger data which are recorded in between beam spills and in dedicated cosmic runs while the beam is off. For the purpose of measuring particle detection efficiencies SMRD counters are divided into two groups, those which are sandwiched by other counters and counters which are in the innermost or outermost radial layers. Efficiencies of counters in the first group can be measured by tagging penetrating cosmic muon with the bracketing counters on either side and determining the fraction for which a muon was observed in the bracketed

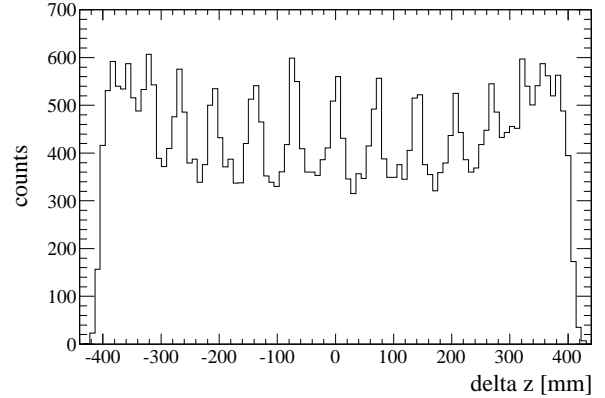


Figure 13: Distribution of estimated hit position  $z_{hit}$  for horizontal counters and cosmic muon data.

layer. The tagging requires each of the two bracketing counters to observe a double ended signal, with individual signal amplitudes larger than 4.5 p.e. and within a coincidence window of 30 ns. The signals of both bracketing counters have to be within a time window of 70 ns to provide a trial event. The ratio of observed events in the sandwiched counter to the total number of trial events is recorded as the detection efficiency of that particular counter. The mean particle efficiency for the 856 counters in category one was found to be  $97.0 \pm 0.4\%$  for horizontal and  $97.9 \pm 0.2\%$  for vertical counters. For counters in the second category a somewhat more sophisticated analysis including track reconstruction is required in order to estimate whether a muon penetrated a given counter in the inner or outermost radial layer. Studies find the detection efficiency for counters in the second category to be comparable to those in the first category. Counter efficiencies are monitored as function of time and are found to be stable within uncertainties.

### 4.4. Detector Stability and Performance

The performance of the SMRD is being monitored by recording the light yield in response to the constant flux of cosmic muons which penetrates the detector. Cosmic trigger data are collected in between beam spills throughout the entire data taking period and during dedicated cosmic muon runs at times when the beam is off. Furthermore, beam data can be used to monitor the SMRD performance if the bunched beam signals are normalized by the number of protons on target (POT) and the uncertainties on the beam are measured by other detectors. Alternatively, if the stability and response of the SMRD is well characterized with cosmic trigger data the SMRD data can be used to provide valuable cross checks on the neutrino beam stability. The present section demonstrates the SMRD performance based on cosmic muon and pre-selected beam data. For the present analysis two cosmic muon data samples were selected, one sample of muons which are vertical to within  $10^\circ$  and a second sample of muons which are horizontal to within  $10^\circ$ . Figure 14 shows good stability in the mean light yield for the vertical and the horizontal cosmic muon samples as function of time. The larger and less stable light yield for vertical

counters during run I is caused by varying trigger settings for the collected data sample of horizontal cosmic muons.

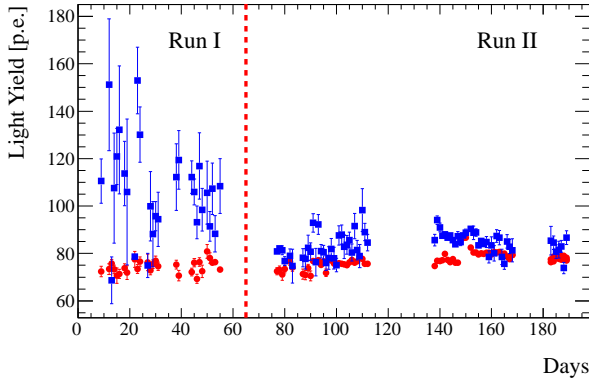


Figure 14: Mean light yield versus time for horizontal (red circles) and vertical (blue squares) SMRD counters in response to cosmic muons penetrating the top and bottom sections of the SMRD.

During the first two run periods from January 2010 to March 2011 the J-PARC accelerator and neutrino beamline delivered  $1.45 \times 10^{20}$  protons on target. After applying beam data quality criteria, a data set corresponding to  $1.43 \times 10^{20}$  POT was identified. The combined duty factor of the SMRD and its data acquisition amounts to 0.97 for the above data taking period. The 6 bunch beam structure used in run 1 (8 bunches for run 2) is clearly visible in the data and displayed in figure 15 which is for an integrated total of  $2.94 \times 10^{19}$  POT. Shown are SMRD

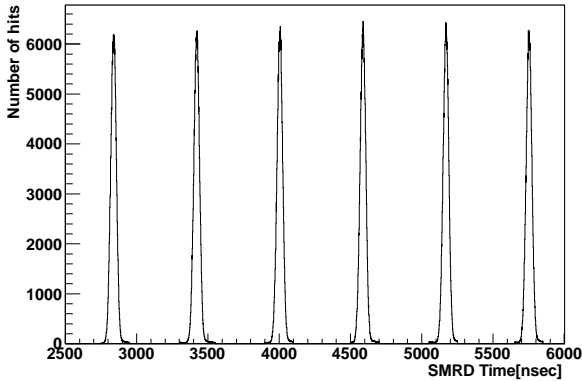


Figure 15: Beam triggered hit time distribution as recorded by the SMRD during run 1 for  $2.94 \times 10^{19}$  POT.

counter hits with a double-sided coincidence. Individual hits contributing to the coincidence are required to have signal amplitudes larger than 10 p.e. and fall within a coincidence window of 23 ns. The electronics integration windows are 430 ns wide and their timing has been adjusted to accept bunch signals in the earlier part of the window. Hence, the later part of each integration window shows random backgrounds as well as a decreasing tail which can be attributed to Michel electrons originating from muon decay. Each integration window is fol-

lowed by a 150 ns dead time of the electronics and the nominal bunch spacing is 581 ns. Beam data collected from March 2010 until March 2011 are used to monitor the SMRD stability over time. The analysis uses double-sided SMRD counter hits (Recon hits) which are composed of single hits on either side of the counter with a charge amplitude greater than 4.5 p.e. and within a 23 ns coincidence window. In addition, the hits are required to fall within a 200ns time window centered on the beam bunches. The rate of background events is estimated from the electronic integration cycles which do not coincide with a beam bunch and is found to be negligible. Nonetheless, background events are subtracted from Recon hits before these are normalized to protons on target (POT). The normalized Recon hits are corrected for temperature and plotted versus time. The temperature dependence of the Recon hit rate is due to the sensitivity of the MPPC overvoltage to temperature as described in [17]. Fig. 16 shows the background subtracted SMRD Recon hits normalized to POT and corrected for temperature effects as function of time. The normalized SMRD Recon hit rate is found to be

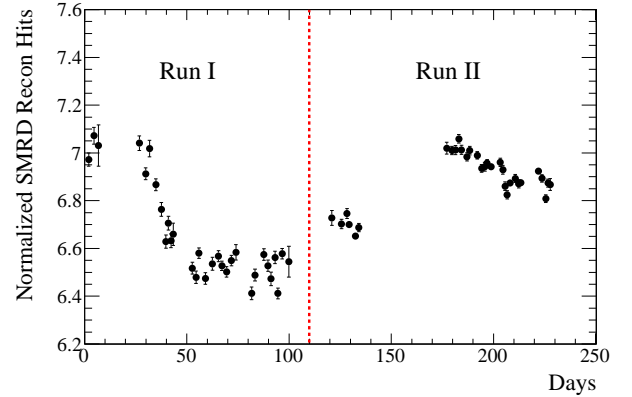


Figure 16: SMRD counter Recon hits normalized by POT and versus time in units of days. The units of the vertical axis are Recon hits per  $1 \times 10^{14}$  protons on target. The error bars reflect statistical uncertainty only.

stable to within 10%.

The SMRD response to cosmic muons has been cross checked with a simulated data set of cosmic muons. The simulation assumes a realistic zenith angle and momentum distribution of cosmic muons on the surface of Earth. It includes the propagation of muons for zenith angles up to  $85^\circ$  through sand in order to reach the detector, the passage of muons through the detector and the creation of electronic hits. The last stage of the simulation is the application of the trigger conditions described in section 3.6. In the simulation the efficiency of the detector and the trigger system was assumed to be 100%. The simulated cosmic muon sample is submitted to the same calibration and reconstruction procedure as the data. A comparison of the angular distributions for data and the simulated sample is shown in Fig. 17 and 18 for an unbiased cosmic ray sample in which all SMRD towers contribute equally to the formation of a trigger. The azimuthal distribution for reconstructed cosmic muon data and corresponding simulation agree within uncertainties. For

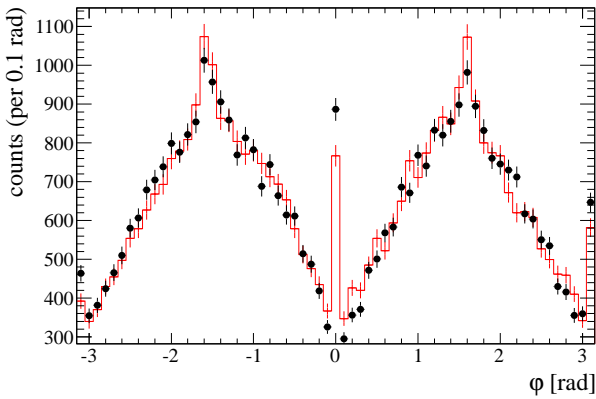


Figure 17: Comparison of the distributions of the azimuthal angle  $\phi$  in data (black points) and simulation (red histogram) for an unbiased cosmic trigger.

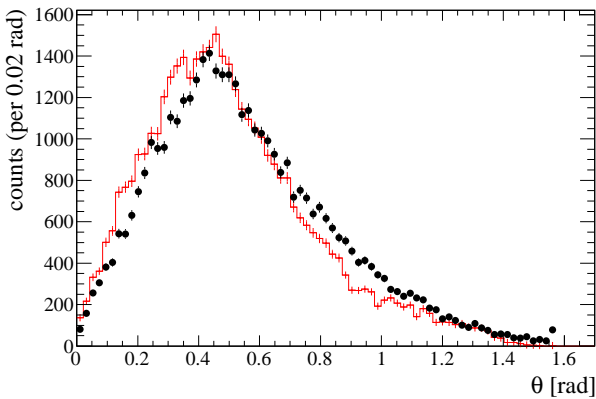


Figure 18: Comparison of the distributions of the zenith angle  $\theta$  based on data (black data points) and simulation (red histogram) for an unbiased trigger configuration.

the zenith angle distribution the reasonable agreement between data and simulation is found and can serve as an indication of the level of understanding of the detector response.

## 5. SMRD Event Reconstruction

A particle track reconstruction in the SMRD is incorporated into the ND280 software package which is designed for physics analyses of ND280 data and to perform detector simulations. The SMRD specific software components consist of a SMRD response simulation, a calibration package and a track reconstruction package solely based on SMRD hit information. Furthermore, a global reconstruction package allows to reconstruct particle interactions inside the detector based on information from all ND280 sub-detectors. The present section gives a brief overview of the event reconstruction algorithms which are based on SMRD information.

The SMRD reconstruction is based on *Recon hits* (“reconstructed hits”) in the SMRD which are built based on time and charge signal information from both sides of the counter and

which take the coordinate in the long direction of the counters into account. The main algorithm used to incorporate SMRD information into the global ND280 reconstruction is a filtering of hits on a hit-by-hit basis. An adjacent track from the ND280 inner sub-detectors is used as a seed and hits from each SMRD wall are tested against it using a Kalman filter [22]. Kalman filtering is performed with the RecPack reconstruction toolkit [23] which handles navigation in magnetic fields, energy loss corrections, multiple scattering and similar processes. The algorithm enables to match even single SMRD hits with high efficiency. A complementary algorithm is the RecPack based matching of inner detector tracks with SMRD tracks which were reconstructed within the SMRD only.

The principal purpose of event reconstruction based solely on SMRD information is to reconstruct tracks from neutrino interactions in the SMRD and which are not matched to any inner detector activity. For beam induced events SMRD activity in opposing sides of the SMRD does generally not originate from single muons. An additional goal is to identify and reconstruct cosmic muons which are used for calibration and detector monitoring purposes.

Since the maximum number of scintillator layers in a tower of the SMRD is six the SMRD-only reconstruction of tracks in one side of the SMRD is based on a small number of hits. In general, a straight line fit is a good approximation to the true particle track in the SMRD. The reconstruction starts with the identification of clusters of hits which is done using hit time stamps and geometrical neighbor criteria. Track fitting is based on the Principal Component Analysis (PCA) [24] method, of which the first component is taken as a fit. For further usage in the global ND280 event reconstruction, SMRD tracks are refitted with the RecPack based Kalman filter in order to obtain covariances.

Individual cosmic muons can produce hits on multiple sides of the SMRD and are used for calibration and performance monitoring purposes. The associated long muon tracks across the ND280 detector are fitted by a PCA method that incrementally removes hits which are located sufficiently far from the initially fitted track. In addition, the possibility exists to match track segments in different SMRD quadrants to form a single long track.

The track finding efficiency of the SMRD only reconstruction algorithm as a function of true muon momentum and cosine of the angle with respect to neutrino beam direction is shown in Figure 19. Neutrino interactions have been simulated within the entire ND280 detector volume. Neutrino energies are derived from a full simulation of the neutrino beam flux [1] and events follow the time structure of the beam. Neutrino interactions are handled by the software package NEUT [26] and secondary particles are propagated and converted to time and charge signals by the custom built GEANT 4 based ND280 software.

## 6. Summary and Conclusion

The elements of the SMRD of the T2K near detector have been described. The construction of the SMRD was completed

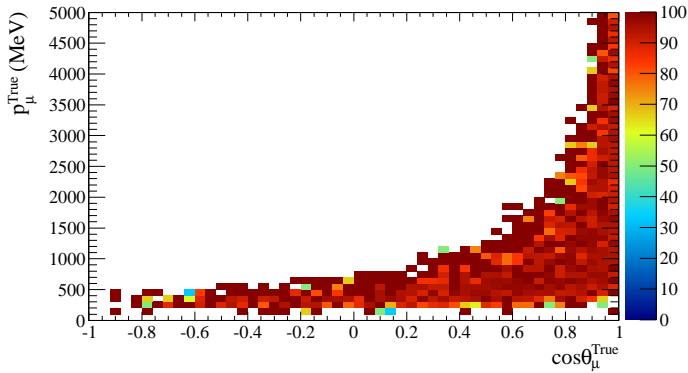


Figure 19: Track finding efficiency of SMRD-only reconstruction for events with at least two muon hits in the detector as a function of true muon momentum and cosine of the angle with respect to the beam direction.

- [17] A. Vacheret et al., Nucl. Instrum. and Meth. A 656 (2011) 69, doi:10.1016/j.nima.2011.07.022; arXiv:1101.1996 [physics.ins-det].
- [18] L. Bellantoni, P. Rubinov, "Bench Test of First TRIP-t Prototypes", D0 note 4845; J. Estrada, C. Garcia, B. Hoenison, and P. Rubinov, MCM II and the Trip chip, D0 note 4009, Fermilab-TM-2226, Dec 2003.
- [19] A. Vacheret et al., Nuclear Science Symposium Conference Record, 2007. NSS '07. IEEE 3 (2007) 1984.
- [20] D.R. Quarrie et al., Comp. Physics Communications 57 (1989) 325 - 331
- [21] Weisstein, Eric W., Moore Neighborhood, From MathWorld-A Wolfram Web Resource. <http://mathworld.wolfram.com/MooreNeighborhood.html>
- [22] R.E. Kalman, J. Basic Eng. 82 (1960) 35; R.E. Kalman, R.S. Bucy, J. Basic Eng. 83 (1961) 95; R. Fruhwirth, M. Regler, Nucl. Instrum. and Meth. A241 (1985) 115
- [23] <http://www.sciencedirect.com/science/article/pii/S0168900204015220>
- [24] C. Holm, ROOT system's TPrincipal class documentation, August 2000, CERN. <http://root.cern.ch/root/html526/TPrincipal.html>
- [25] S. Ritt, P. Amaudruz, K. Olchanski, MIDAS (Maximum Integration Data Acquisition System), 2001. <http://midas.psi.ch>.
- [26] Y. Hayato, Nucl. Phys. (Proc. Suppl.) 112 (2002) 171.

in summer of 2009 and followed by a successful commissioning phase. The performance of the SMRD was evaluated with cosmic ray data and found to meet or exceed specifications. The detector response to cosmic muons was analyzed and found to agree with simulations. T2K started taking neutrino beam data for physics analysis in January 2010.

### 6.1. Acknowledgements

The authors thank the Department of Energy, U.S.A.; the Russian Academy of Sciences, the Russian Foundation for Basic Research, and the Ministry of Education and Science of the Russian Federation, Russia; the Polish National Science Centre, Poland; and the Science and Technology Facilities Council, U.K. In addition, the participation of individual researchers and LSU in the construction of the SMRD has been further supported by funds from the U.S. Department of Energy Outstanding Junior Investigator (OJI) Program.

## References

- [1] K. Abe et al., (The T2K Collaboration) Nucl. Instrum. and Meth. A 659 (2011) 106, doi:10.1016/j.nima.2011.06.067; arXiv:1106.1238 [physics.ins-det].
- [2] K. Abe et al., (The T2K Collaboration) arXiv:1201.1386 [hep-ex]. K. Abe et al., (The T2K Collaboration) Phys. Rev. Lett. 107 (2011) 041801, arXiv:1106.2822 [hep-ex].
- [3] S. Machida, Nucl. Phys. (Proc. Suppl.) B 155 (2006) 58.
- [4] Y. Fukuda et al., (The SuperKamiokande Collaboration) Nucl. Instrum. and Meth. A 501 (2003) 418.
- [5] T. Le, arXiv:0910.4211v1 [hep-ex].
- [6] Yu. Kudenko, Nucl. Instrum. and Meth. A 598 (2009) 289.
- [7] T2K ND280 Conceptual Design Report, T2K Internal Document.
- [8] O. Mineev et al., Nucl. Instrum. and Meth. A 577 (2007) 540.
- [9] K. Nakamura et al. (Particle Data Group), J. Phys. G 37 (2010) 075021.
- [10] T2K Collaboration, K. Matsuoka, talk at TIPP09 Conference, Tsukuba, Japan, 2009.
- [11] T2K Collaboration, A.K. Ichikawa, Proc. of the Int. Conf. on Topics in Astroparticle and Underground Physics, Gran Sasso, Italy, 2009.
- [12] A. Ivashkin et al., Nucl. Instrum. and Meth. A 394 (1997) 321.
- [13] Yu. Kudenko et al., Nucl. Instrum. and Meth. A 469 (2001) 340.
- [14] N. Yershov et al., Nucl. Instrum. and Meth. A 543 (2005) 454.
- [15] Kuraray Co. Ltd. Scintillation materials catalogue.
- [16] Yu. Kudenko et al., PoS PD07 (2007) 016.